Future Mesh-Networked Pico Air Vehicles

Daniel S. Drew, Brian Kilberg
and Kristofer S. J. Pister
BSAC, University of California, Berkeley
Email: ddrew73@berkeley.edu

Abstract—Taken together, recent advances in microelectrome-chanical systems, wireless mesh networks, digital circuits, and battery technology have made the notion of autonomous pico air vehicles viable. In this work we describe the core technologies enabling these future vehicles as well as propose two possible future platforms. We draw on recent research on high thrust density atmospheric ion thrusters, microfabricated silicon control surfaces, and extremely low mass and power mesh networking nodes. Using the same open-source network implementation as we have already demonstrated in larger UAVs, these flying microrobots will open up a new application space where un-obtrusiveness and high data granularity are vital.

I. INTRODUCTION

Wireless mesh networking has the potential to connect swarms of hundreds or thousands of Unmanned Aerial Vehi-cles (UAVs) across size scales from meters down to millime-ters. Early funding for low-power wireless mesh networking was provided by DARPA to demonstrate autonomous aerial deployment of sensors via UAV in 2001 [1] (Figure 1). Since then, academic research, commercial developments, and international standardization have created a powerful set of tools for future swarms [2].

Microelectromechanical systems (MEMS) technology con-tinues to drive down the size, power, and cost of the inertial sensors necessary for stable flight, and smartphone markets continue to drive down the size, power, and cost of digital computation and mission-related sensors (e.g. camera, micro-phone) as well as improve the energy and power density of batteries. Taken together with the improvements in networking, this means that the mass of a minimum useful payload for autonomous or semi-autonomous UAV operation has fallen from kilograms, to grams, to milligrams today. We believe that for many applications, the size of a useful and practical UAV will shrink down to a scale of centimeters or less.

Indeed, a decade after the meter-scale UAV in Figure 1 deployed its sensor mesh and tracked its targets, a ten-times smaller, one thousand times lighter UAV (Figure 2) performed a similar mission. Flying into a building with a payload of three mesh network enabled sensors, the copter was remotely piloted via radio commands sent in over the mesh network that it was deploying itself. Two images per second were relayed out over the network to the operator [3], and control information was sent into the network at a rate of several commands per second. As the copter progressed into the building it dropped its sensor/relay nodes one by one in order to maintain network connectivity [4].

Fig. 1. Autonomous UAV with 8 wireless mesh sensors in exterior "bomb bay". Sensors were dropped at specific GPS locations, where they formed a mesh network, shared data about vehicle magnetic events, and relayed summary track information to the UAV each time it returned and joined the network. The UAV then relayed that information to the ground station on its next overflight [1].
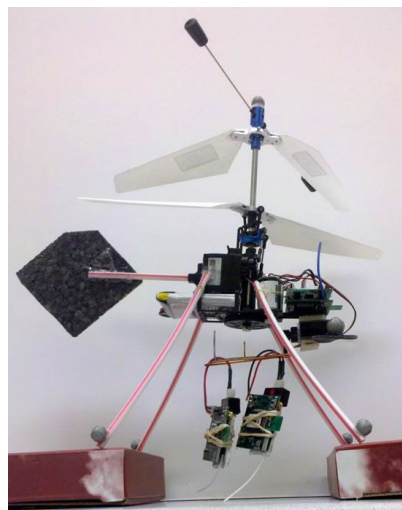

Fig. 2. A remote-piloted 15cm copter carrying two droppable mesh network-ing relay/sensor nodes. Images from the copter were relayed out over the mesh network, and flight commands were relayed in. The copter dropped sensors as needed to maintain network connectivity as it flew into a building [4].

Recent results in MEMS devices for propulsion and aerodynamic control give reason to believe that a reduction of another order of magnitude in size, and three orders of magnitude in mass, for autonomous and semi-autonomous UAVs may soon be achievable.

Micro aerial vehicles (MAVs) have already emerged as a viable subclass of UAVs, with an application space including search and rescue [5] and aerial photography [6]. However, the tradeoff between vehicle size and capability has seemed to have stalled progress developing novel application spaces for small, cheap UAVs. Relatively recent research on pico air vehicles, defined as having a maximum dimension of 5cm or less and a maximum takeoff mass of 500mg or less, aims to push the boundaries of unobtrusive, low unit-cost autonomous vehicles to the point where we can use them as disposable, versatile swarms [7].

The common propeller-based designs used in the majority of commercial UAVs begin to fail at the centimeter scale with decreased flight time, durability, and aerodynamic stability. As a result, successful work in this sphere has largely been biomimetic, specifically seeking to replicate the flapping wing flying mechanism of insects such as the bee. While many of these systems have demonstrated impressive performance, their complexity can make them difficult to design and build and their thrust to weight ratio at a centimeter scale is not much greater than one [8]. Current models do not have the payload capacity to use commercial off-the-shelf sensors (COTS) and instead have turned to the development and integration of research-grade devices, sometimes themselves biomimetic [9].

By developing a pico air vehicle that uses mechanisms with no natural analogue for propulsion we hope to expand the design space beyond that dictated by flapping wing flight. One proposed platform will instead have fixed wings, use electrohydrodynamic (EHD) thrust for propulsion, and use MEMS-based surfaces for stability and control. Thrust to weight ratio will be high enough to use COTS sensors, and along with an ultra low power system-on-a-chip and printed thin-film batteries, will be able to fly autonomously. While the lift to drag ratio afforded by fixed wing geometries does decrease at the low Reynolds numbers (about 1e4) relevant to pico air vehicles, previous research has demonstrated ratios in excess of 10 from centimeter-scale wings [10]. Compared to a flapping wing mechanism, fixed wing designs are simple to design, do not require as much materials engineering, and can be built for durability. EHD thrusters are silent, have a high thrust to weight ratio due to requiring only sparse electrodes to produce useful work, and are mechanically robust due to their lack of moving parts [11]. Another potential platform is the microrocket. Previous work on millimeter-scale rocket motors has yielded thrusts of up to 20mN with 40 second burn times [12], which could enable controlled long range flight with the same onboard electronics package.
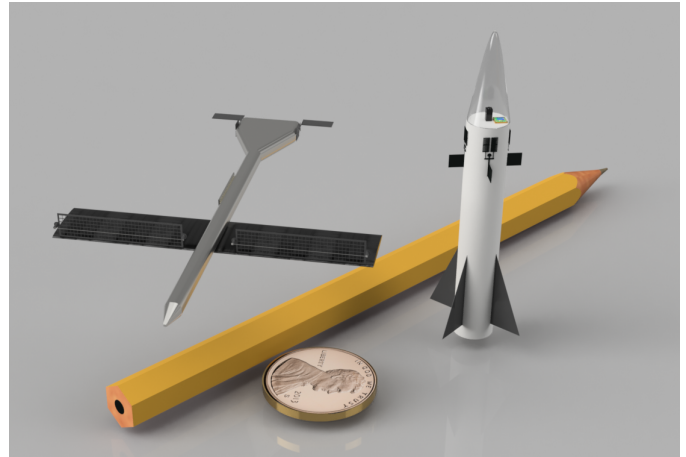

Fig. 3. Rendered depictions of the proposed pico air vehicle platforms. On the left is an atmospheric ion thruster powered fixed wing vehicle and on the right is a controllable millimeter-scale rocket.

II. Contributing Technologies

A. Networking

Ad hoc wireless mesh networking is difficult, and remains an active area of academic research and commercialization. A combination of IEEE and IETF standard protocols provides one flexible approach to low-power, high-reliability, low data rate ad hoc mesh networking. OpenWSN is an open-source implementation of that collection of standards [2]. Based on the 2.4 GHz, 250 kbps IEEE 802.15.4 physical layer, the 802.15.4E TSCH time-synchronized channel-hopping medium access layer, and the IETF 6TiSCH, 6LoWPAN, RPL, and CoAP standards for IPv6 support, routing, and applications, OpenWSN provides a simple and popular software framework that runs on more than a dozen low-cost platforms [13]. All nodes in an OpenWSN network maintain a shared sense of time accurate to a fraction of a millisecond, while maintaining a baseline radio duty cycle of less than 1%. On commercially-available hardware, this corresponds to average current levels on the order of $10\mu A$ from a 3V supply, a negligible power consumption for most UAVs. Radio transmission and reception is synchronized, with a 100 byte payload sent and received in roughly 4ms. Peak current consumption during active radio use is roughly 10mA depending on the specific commercial hardware. The power consumption of a node in the network depends on the amount of traffic that it generates, terminates, and that it routes for its neighbors. Models of in-network power consumption based on measured charge consumption of elementary operations (packet TX, packet RX, unused RX opportunity) combined with network utilization (packets/second, route/network topology) yield accurate predictions of performance [14]. A network of hundreds of UAVs broadcasting periodic position updates to each other might cost 0.1mW on each UAV to do so, whereas sending imagery at maximum rate would push the nodes involved to 10mW or more [3].

The smallest platforms able to run OpenWSN to date are in the GINA (Guidance and Inertial Navigation Assistant) fam-
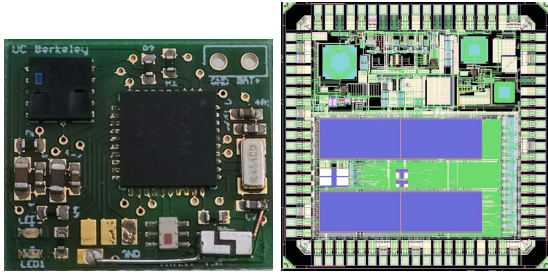
Fig. 4. Current and future mesh sensor nodes. Left: Mimsy, a 1.5cm by 1.7cm, 1 gram wireless sensor node. Right: Layout of a 4mm^2, 5mg chip with 32 bit microprocessor, 128kB of SRAM, and a 2.4 GHz transceiver.
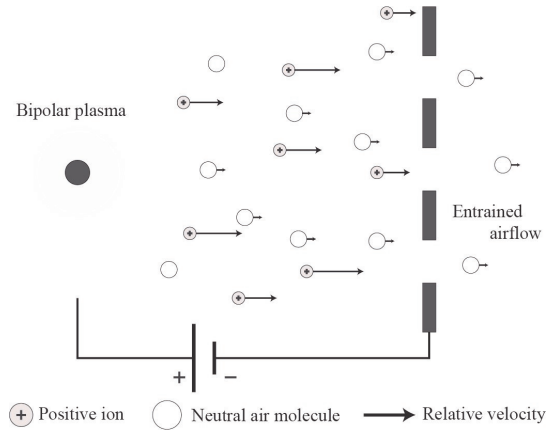

Fig. 5. In a positive corona discharge, geometrically asymmetric electrodes result in local field enhancement around the emitter. At some critical field, Townsend ionization results in a sustained bipolar plasma. Positive ions drift in the electric field to the collector. Along the way, they collide with neutral molecules and transfer momentum.

ily [15], the latest and smallest of which is shown in Figure 4. This platform contains the radio and microprocessor chip, 9-axis IMU, two external crystal oscillator frequency references, chip antenna, infrared proximity sensor, and associated passive components.

Recent work has shown that significant reduction in the size and cost is possible. Using only on-chip time and frequency references it will soon be possible to build a chip that will run OpenWSN and join a time synchronized channel hopping mesh network [16]. Removing the need for external real-time clock crystal [17] and RF crystal [18] references reduces the size, power, and cost of the mesh networking nodes. As shown in Figure 4, the first attempt at such a chip is only $2mm^3$ and weighs 5mgm, roughly the same as the IMU chip. Testing is still underway. Simulations indicate that the processor and SRAM should consume $30\mu A/MHz$ [19], and the radio should be significantly lower power than those in existing commercial platforms supported by OpenWSN.
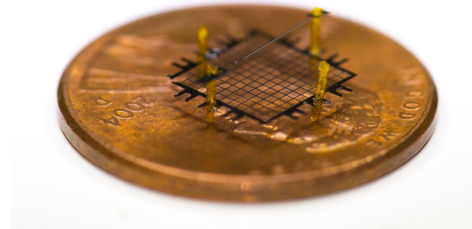

Fig. 6. A hand-assembled atmospheric ion engine, made of microfabricated silicon active electrodes and fused silica capillary tubes as dielectric standoffs. This 6mg device has a thrust to weight ratio of over 20 [11].

B. Atmospheric Ion Engines

Thrust will be produced electrohydrodynamically, that is, by collisions between charged and neutral particles resulting in a net directional momentum transfer. Since the momentum transfer is more efficient when the charged particles are ions instead of electrons, the neutral gas flow produced via EHD devices is often referred to as an ion wind. A common method for producing the ions is corona discharge, which has been adopted for commercial applications including electrostatic precipitators and mass spectrometers. The mechanism of corona discharge induced ion wind is illustrated in Figure 5.

Derivations of EHD thrust, efficiency, and induced air flow velocity are typically simplified with the following assumptions: gas and ion parameters are uniform across the thruster; high ion drift velocity relative to inlet air velocity; and constant ion mobility within the induced space charge [20]. This leads to a simple set of equations describing the relationships between applied electric field, E, ion (corona) current, I, and force, F:

$$F = \beta \frac{Id}{\mu} \qquad (1)$$

$$\frac{F}{P} = \frac{d}{\mu V} = \frac{1}{\mu E} \qquad (2)$$

Where d is the separation between the electrodes, μ is the ion mobility in air (about 2 cm^2/Vs), and β is a loss factor that is a function of electrode geometry.

We have previously demonstrated microfabricated EHD thrusters generating over $10N/m^2$, with thrust to weight ratios over 20 and thrust densities of over $1000N/m^3$ (see Figure 6) [11]. A peak outlet air velocity of over $4m/s$ was measured (Figure 7), consistent with prior research measuring centimeter-scale EHD thrusters [21]

The first steps towards controlled flight of a flying microrobot using EHD thrusters have been taken, with demonstrated takeoff and rudimentary control over attitude by selectively actuating individual thrusters [22]. After accounting for the airframe the thrust to weight ratio decreased to around 10, giving the 1.8cm by 1.8cm microrobot a payload capacity of about 90mg.
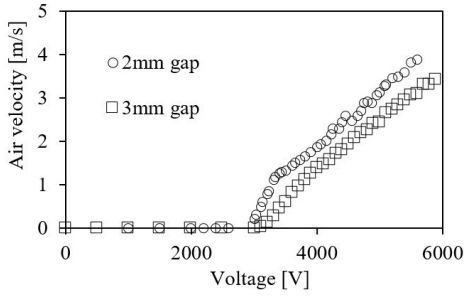
Fig. 7. Applied voltage vs airflow for a 6.5mm x 6.5mm outlet ion engine [11].
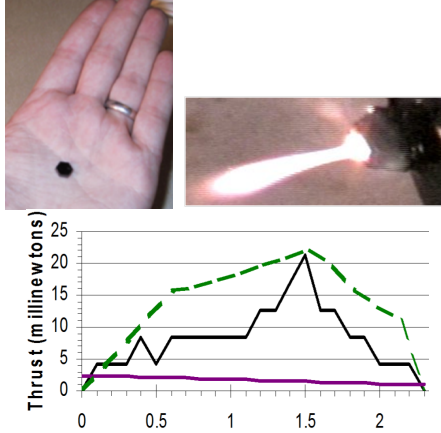

Fig. 8. Millimeter-scale rocket motor. Top left: assembled rocket motor; Top right: ignition on the test stand; Bottom: simulated thrust (green), measured thrust (black), and rocket weight (purple) vs. time in seconds.

C. Millimeter-scale Rocket Propulsion

In previous work [23] we have demonstrated that a rocket motor smaller than a dime can produce enough thrust over time to fly 50m straight up, and hundreds of meters horizontally. The 8mm diameter 2.5mm thick rocket contained roughly 100mgm of AP/HTPB propellant, and achieved an I_{SP} of roughly 25 (Fig. 8). More recently, work at Harvard has shown a 3mm diameter 4cm long rocket motor with 5mN of thrust for 25 seconds [12], and an I_{SP} of 27 seconds. This group also demonstrated a 6mm diameter, 6cm long motor that could produce 20mN of thrust for 40 seconds. These motors could lift millimeter-scale rocket systems that weigh up to 2g.

D. Microfabricated Control Surfaces

MEMS are devices microfabricated using processes adapted from the semiconductor industry that can perform a variety of useful functions. For example, inertial measurement units (IMUs), radio frequency filters, and certain pressure sensors are based on MEMS technologies. The feature sizes of these devices can be on the order of 1 μm. Electrostatic gap-closing actuators are one example of MEMS that are used to drive resonators and gyroscopes. While these actuators have useful force performance on the microscale, they are limited by their small maximum displacement [24]. Electrostatic inchworm
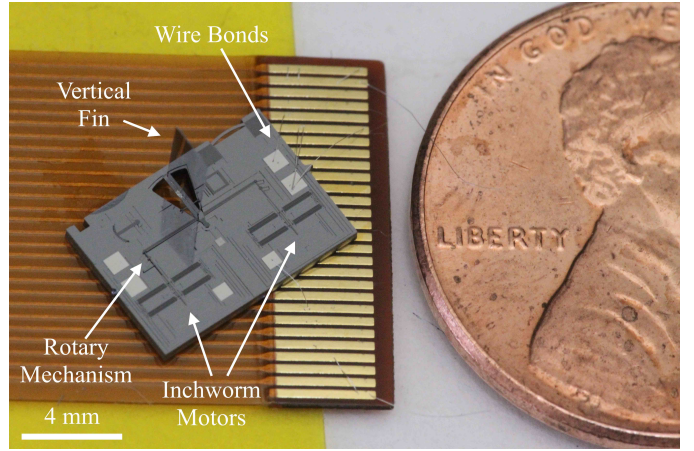

Fig. 9. Assembled MEMS control surface. After fabrication, a vertical fin is inserted into the planar silicon mechanism and epoxied into place. The device's electrical pads are then wire-bonded to solderpads, where power tether wires can be soldered. The size of the chip is 9mm x 7mm x 0.59mm.

motors solve this problem by repeatedly driving a pair of electrostatic gap-closers with a clutch mechanism, allowing large linear displacements while preserving the force output of the gap closers [25] [26]. These motors have force densities of up to $2\frac{mN}{mm^2}$ [26]. Previous work in our group has demonstrated planar silicon pin joints that can be used to design mechanisms that translate linear actuation into more complicated rotations and trajectories [27]. Researchers have demonstrated the ability of these motors to actuate millimeter-scale robots [28] [29].

We used electrostatic inchworm motors and silicon pin joints to design a MEMS aerodynamic control surface. They are manufactured in a two-mask silicon-on-insulator (SOI) process. This process was also used by our group to design silicon pin joints and inchworm motors in the past [27] [29]. The final thickness of the device is 590μm. Figure 9 shows the fully assembled and fabricated control surface. The inchworm motors drive a planar pin-joint assembly that causes a rotation in a fin.

These control surfaces have a current as-fabricated mass of 73mg. However, this weight could be further reduced; at least 50% of the substrate area is unnecessary to the design and could be etched away. Additionally, reducing the 550 μm substrate to a thickness of 100 μm could be accomplished without adversely affecting the operation of the control surfaces. This would result in a 50% reduction in area and a 76.2% reduction in thickness. After these size reductions, the control surfaces would have a mass of 8.7mg.

The maximum torque specification of the control surfaces is determined by the amount of aerodynamic forces they need to sustain. In this case, Equation 3 approximates the experienced lift forces on the fin that has an area of A_{ref}, angle of attack of α, an airspeed of V, and is inside a gas of density ρ. This assumes that the $|\alpha| < 15°$. This force is experienced at the quarter chord of the fin.

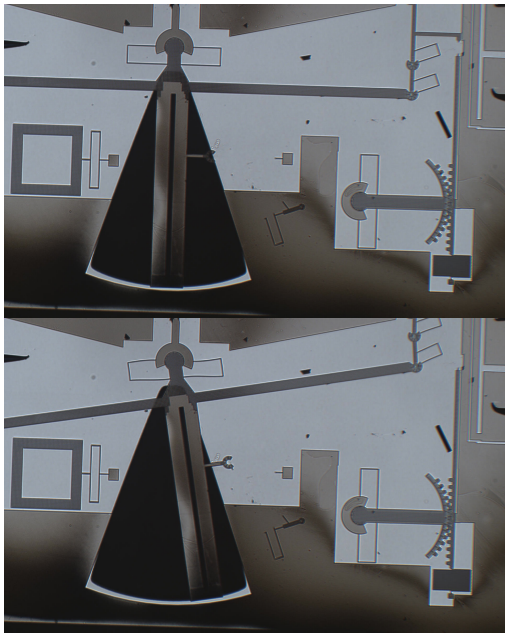$$F_{lift} = \frac{1}{2}\rho V^2 2\pi \alpha A_{ref} \quad (3)$$

Fig. 10. Demonstration of a microfabricated control surface actuating. The maximum deflection observed was 10 degrees. In this figure, the fin has not been inserted into the slotted arm yet.

Fig. 11. An assembled control surface under 5 degrees of deflection. The fin is the mirrored surface protruding vertically from the chip.

With force densities of $2\frac{\text{mN}}{\text{mm}^2}$, the inchworm motors should be able to provide enough force to maintain aerodynamic forces in the mN range. Measured results from static loading and dynamic actuation of the fin shown in Figure 9 have shown a peak force of 1.5mN at 1/4 chord, a +/-10 degree actuation range, and an unloaded rotation rate of 100 degrees/second.

The demonstrated operating voltage of these control surfaces is 40V-110V [30], with output force of the inchworms proportional to the square of the operating voltage. The estimated capacitance of an inchworm motor array is about 5pF [26]. In order to drive one step of actuation in the inchworm this capacitance must be charged up to 80V, which requires about 32nJ. In order to run the inchworms at 1000Hz, this capacitance must be charge 1000 times per second, which yields 32μW of power. We have demonstrated operating frequencies of over 3000Hz [30], which corresponds to a maximum rotation rate of over 100 degrees/second.

E. High-Voltage Circuitry

The control surfaces will require voltages on the order of 100V and the thrusters will require voltages on the order of 1000V. A method of supplying, switching, and modulating this voltage must be integrated with the vehicle. Previous work has demonstrated SOI CMOS circuits with NMOS breakdown voltages above 50V and PMOS close to 100V working alongside similar mechanisms to the control surfaces shown here [31]. For the EHD thrusters these transistor breakdown voltages could be increased further with process optimization or worked around in circuit design. Multi-junction solar cell arrays, fabricated on SOI wafers alongside the aforementioned MEMS structures and CMOS circuits, have been demonstrated
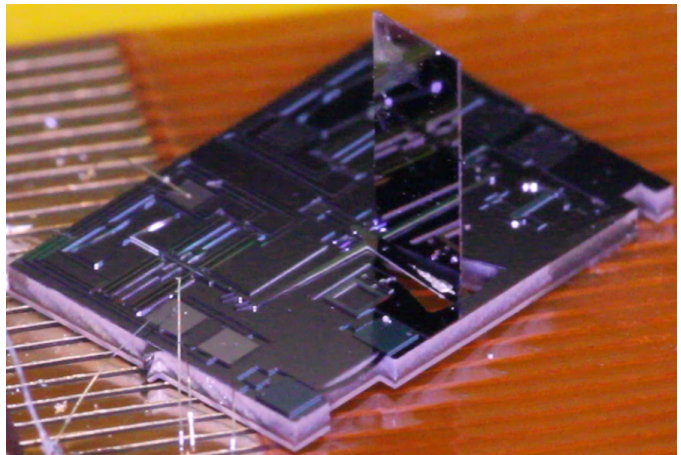
with efficiencies greater than 11% and output voltages above 80V [28]. Theoretically this output voltage can be increased by increasing the number of cells in the series bank, although the thickness of the cells and the low open circuit voltage make them non-ideal candidates for a highly mass-constrained EHD flier.

III. FUTURE PLATFORMS

This section discusses two potential mobility platforms for future pico air vehicles as well as an electronics payload that they could both make use of.

A. Electronics Package

Prior work has demonstrated an open source guidance and inertial measurement unit (GINA) for use in autonomous MAVs [15]. The 6 square centimeter, 1.6 gram board contained a commercial 9-axis IMU, microprocessor, and 2.4GHz wireless radio. Using an inkjet printed circuit board on a $25\mu m$ thick plastic substrate [32], a COTS 9-axis IMU, a 250x250 pixel CMOS imager, and the system on a chip described in a previous section running OpenWSN, we aim to create a sub 100mg successor to GINA for use in autonomous pico air vehicles. A quarter wavelength antenna extending along the fuselage will enable wireless communication. A 2.3mg, 50V solar cell array and accompanying high voltage buffer circuit fabricated in an SOI process has been previously demonstrated [28]. We will assume a fabricated mass of 5mg for a switching circuit operating at the higher voltages necessary for the ion thrusters.

B. Ion Jet Plane

The vehicle will be designed similarly to a training glider, with a long fuselage providing stability for thin airfoils. It will use two MEMS elevons mounted on the tail to control pitch and roll. Yaw can be controlled by differential actuation of the wing-mounted thrusters. The ion thrusters will be placed along the leading edges of the wings. An approximate design is depicted in Figure 3. Previous work on an elevon-controlled

MAV glider found lift to drag ratios in the range of five to ten from a 10cm-span airfoil operating at a Reynolds number of around 7000 [33]. Until wind tunnel measurements are performed using sample airfoils we will base our design on an estimated lift to drag ratio of five. Assuming the same thickness of airfoil and fuselage material as in [33] but halving the area, we can assume a combined airfoil and fuselage mass of about 100mg. Each microfabricated control surface can be brought to about 8mg with process optimization. The electronics package will be mounted on the side of the fuselage, close to the center of mass.

Assuming we want to operate at a thrust efficiency of $10mN/W$, our operating drift field from Equ. 2 will be $500kV/m$ and our theoretical thrust from Equation 1 is therefore approximately $2.5N/m^2$; a four-fold reduction in thrust from [11]. For our vehicle mass of 216mg and an estimated lift to drag ratio of 5 we require about $400\mu N$ of EHD force. With thin film lithium cobalt oxide - graphite batteries ([34]) that have a power density of $1W/g$ and our thrust efficiency of $10N/W$ we require about 40mg of battery. Assuming an aerial energy density of $1.4J/mm^2$ without packaging, this means we need about 150 square millimeters of battery for a flight time of one hour. If the thrust to weight ratio of our ion thrusters scales proportionally to the decreased drift field we can expect a ratio of about 5; this means we will need a minimum of about 60mg and 240 square millimeters of thruster, producing about $600\mu N$ of force, for a total 1:1 vehicle thrust to weight ratio. For maneuvering, the drift field of the thrusters can be increased at the cost of efficiency and therefore flight time.

C. Millimeter-scale Rocket

Viable thrust methods have been demonstrated for millimeter-scale rockets and were previously mentioned in this paper [12]. For example, using the motors from [12], we could have up to 40 seconds of thrust at 20mN in a 6mm x 6cm package. These motors approached impulse to mass ratios of 1Ns/g. A 20mN average thrust would give us a weight budget of 2g to allow for vertical flight. The fuselage weight would be dominated by the weight of the motor, which for 40 second burn times at 20mN would be 750mg. Extra structural weight for payload bay and fins is assumed to be 100mg.

The microfabricated control surfaces would be located on the rocket as canards. Four of these would be required to fully control the roll, pitch, and yaw of the rocket. Using the previous maximum estimate on inchworm power consumption of 32 μW, the total power consumption of these is 128 μW.

DC-DC converters have been used previously on microgliders to provide high voltages for piezoelectric actuators [33]. A COTS boost/charge pump converter, the Linear Technologies LT3482, has a 3mm x 3mm footprint and can provide up to 5mA at 90V. It's quiescent power consumption is 9mW when not connected to a load. This integrated circuit could be easily used as the actuator power source.

The total power consumption of this system is about 15mW, as detailed in Figure 12. For up to a minute of fly time, we would require only 0.24mWh of battery capacity to operate the system. Assuming an aerial energy density of $1.4J/mm^2$ for the batteries we would only need $0.63mm^2$ of battery area to sustain operation for 60 seconds. We will assume the battery weight would be 40mg. Figure 12 also summarizes the mass of the millimeter-scale rocket system.

	Power Consumption (mW)	Mass (mg)
Fuselage	N/A	100
Inchworm Motors	0.128	35
SCuM	0.200	2
Camera	4.2	4
IMU	1.1	14
Rocket Motor	N/A	750
Batteries	N/A	40
LT3482	9	16
Total	14.628	961

Fig. 12. Table summary of mass and power consumption of millimeter-scale rocket system.

We simulated an 6mm diameter, 6cm long, 1g rocket that was powered by the 20mN rocket motor shown in [12]. We estimated the inertial tensor of the rocket by approximating it as a solid cylinder which is given in Equation 4.

$$I = \begin{bmatrix} \frac{1}{12}mh^2 + \frac{1}{4}mr^2 & 0 & 0 \\ 0 & \frac{1}{12}mh^2 + \frac{1}{4}mr^2 & 0 \\ 0 & 0 & \frac{1}{2}mr^2 \end{bmatrix} \quad (4)$$

We modeled the force generated by the control surfaces and stabilizing fins with Equation 3. The four control surfaces were 2mm x 4mm canards that were located 2cm from the center of gravity of the rocket. The canards were spaced rotationally by $90°$ around the fuselage. The the aerodynamic drag of the rocket was estimated using OpenRocket, an open source simulation tool used for model rocketry design. We used the MATLAB Simulink Aerospace Blocket to implement a body dynamics simulation of the rocket. We controlled the rocket using three 2-degree-of-freedom (2DOF) PID controller blocks that each tracked the desired pitch, yaw, and roll angles separately. The outputs of the three controllers were mapped to the angles of attack of the four canards. During simulation, the forces experienced by the control surfaces at the quarter chord were under 10mN, which means they can be supported by our MEMS control surfaces if we increase their inchworm motor area and mechanical advantage. The maximum speed of the simulated rocket was 67m/s and its tightest turning radius was roughly 20m. Figure 13 illustrates the simulated trajectory of this rocket.

IV. OPEN PROBLEMS

A. Integration and Assembly

Previous efforts to integrate MEMS mechanisms, high voltage SOI solar cell arrays and buffers, and CMOS sequencers resulted in large parasitic losses [28]. Reproducible assembly of microfabricated components is an active area of research. Current hand-assembly techniques are relatively slow and have insufficient yield for the complicated platforms described
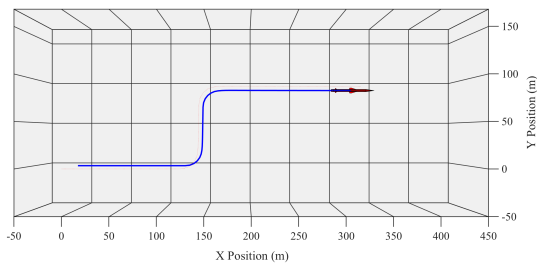
Fig. 13. Simulated maneuver of a 6mm diameter, 6cm long rocket. The simulated rocket was powered by a 20mN thrust millimeter-scale rocket motor and was controlled by control surfaces resembling our MEMS control surfaces. The turning radius of the maneuvers was approximately 20m. This simulation was stopped after the first 8 seconds of flight.

herein. Recent work has demonstrated chip-level assembly of a complicated structure using a combination of external fixtures and guides built into the microfabricated components [35]. This structure also provided for electrical routing without external wire bonds. Extra care must be taken in our case to provide isolation for the high voltage lines for the ion thrusters and control surfaces. We propose to accomplish this with a combination of deliberate routing and deposition of a conformal dielectric film (e.g. Parylene).

B. Thin-Film Batteries

One of the challenging aspects of the battery integration process is obtaining a hermetic seal in the dozens of millimeter-scale battery cavities necessary for the voltages required. A suitable combination of surface treatment, higher pressures, rapid thermal processing, and dispensed adhesives will be required. The printing process has to be controlled to minimize variations in material loading and electrode geometry between the cells, as differences in capacity or performances of individual cells can lead to overcharging and premature failure of the battery array.

V. Conclusions

We have presented some of the core technologies that will enable a new class of UAV, the pico air vehicle. Our assertion is that recent advancements on a number of fronts will lead to platforms with the same or greater capabilities as current MAVs with an order of magnitude smaller critical dimension. They may be used in concert with other autonomous vehicles in cooperative fleets [36], as coordinated tools for assembly of other robots or larger structures [37], or even as interface elements that can interact with humans in novel ways [38] [39].

Acknowledgment

References

[1] K. Pister, "Air-dropped fixed/mobile wireless sensor network," March 2003, marine Corps Air/Ground Combat Center, Twentynine Palms, CA http://robotics.eecs.berkeley.edu/~pister/29Palms0103, retrieved Feb 10, 2017.

[2] T. Watteyne, X. Vilajosana, B. Kerkez, F. Chraim, K. Weekly, Q. Wang, S. Glaser, and K. Pister, "Openwsn: a standards-based low-power wireless development environment," *Transactions on Emerging Telecommunications Technologies*, vol. 23, no. 5, pp. 480–493, 2012.

[3] T. Watteyne, F. Chraim, N. Sarmicanic, C. Jian, and K. S. Pister, "Video transmission over a standards-based wireless multi-hop sensor network," *E-LETTER*, 2010.

[4] A. Mehta, T. Watteyne, and K. Pister, "Image transmission and vehicle control through buildings via a drop-off-mote mesh network," 2001, Army MAST program Joppa Demo (unpublished).

[5] T. Tomic, K. Schmid, P. Lutz, A. Domel, M. Kassecker, E. Mair, I. L. Grixa, F. Ruess, M. Suppa, and D. Burschka, "Toward a fully autonomous uav: Research platform for indoor and outdoor urban search and rescue," *IEEE robotics & automation magazine*, vol. 19, no. 3, pp. 46–56, 2012.

[6] D.-R. C. How, B. A. Barbarich-Bacher, and K. A. Stol, "Design and analysis of a uav for skydiving," in *Unmanned Aircraft Systems (ICUAS), 2015 International Conference on*. IEEE, 2015, pp. 348–355.

[7] R. J. Wood, B. Finio, M. Karpelson, K. Ma, N. O. Pérez-Arancibia, P. S. Sreetharan, H. Tanaka, and J. P. Whitney, "Progress on picoair vehicles," *The International Journal of Robotics Research*, vol. 31, no. 11, pp. 1292–1302, 2012.

[8] R. J. Wood, "The first takeoff of a biologically inspired at-scale robotic insect," *IEEE transactions on robotics*, vol. 24, no. 2, pp. 341–347, 2008.

[9] P.-E. J. Duhamel, N. O. Pérez-Arancibia, G. L. Barrows, and R. J. Wood, "Biologically inspired optical-flow sensing for altitude control of flapping-wing microrobots," *IEEE/ASME Transactions on Mechatronics*, vol. 18, no. 2, pp. 556–568, 2013.

[10] P. J. Kunz, "Aerodynamics and design for ultra-low reynolds number flight," Ph.D. dissertation, Stanford University, 2003.

[11] D. Drew, D. S. Contreras, and K. S. J. Pister, "First thrust from a microfabricated atmospheric ion engine," in *Micro Electro Mechanical Systems (MEMS), 2017 30th IEEE International Conference on*. IEEE, 2017.

[12] M. Kovac, M. Bendana, R. Krishnan, J. Burton, M. Smith, and R. J. Wood, "Multi-stage micro rockets for robotic insects," *Robotics: Science and Systems VIII*, p. 185, 2013.

[13] "http://openWSN.org."

[14] X. Vilajosana, Q. Wang, F. Chraim, T. Watteyne, T. Chang, and K. Pister, "A realistic energy consumption model for tsch networks," *IEEE Sensors Journal*, vol. 14, no. 2, pp. 482–489, 2014.

[15] A. M. Mehta and K. S. Pister, "Warpwing: A complete open source control platform for miniature robots," in *Intelligent Robots and Systems (IROS), 2010 IEEE/RSJ International Conference on*. IEEE, 2010, pp. 5169–5174.

[16] B. Wheeler, F. Maksimovic, N. Baniasadi, S. Mesri, O. Khan, D. Burnett, A. Niknejad, and K. Pister, "Crystal-free narrow-band radios for low-cost IoT," in *RFIC, to appear*, 2017.

[17] O. Khan, B. Wheeler, D. Burnett, F. Maksimovic, S. Mesri, K. Pister, and A. Niknejad, "Frequency reference for crystal free radio," in *Frequency Control Symposium (IFCS), 2016 IEEE International*. IEEE, 2016, pp. 1–2.

[18] O. Khan, B. Wheeler, F. Maksimovic, D. Burnett, A. Niknejad, and K. Pister, "Modeling the impact of phase noise on the performance of crystal-free radios," *IEEE Transactions on Circuits and Systems II*, Sept. 2016.

[19] S. Mesri, "Design and user guide for the single chip mote digital system," Master's thesis, EECS Department, University of California, Berkeley, May 2016. [Online]. Available: http://www2.eecs.berkeley.edu/Pubs/TechRpts/2016/EECS-2016-71.html

[20] L. Pekker and M. Young, "Model of ideal electrohydrodynamic thruster," *Journal of Propulsion and Power*, vol. 27, no. 4, pp. 786–792, 2011.

[21] E. Moreau, N. Benard, J.-D. Lan-Sun-Luk, and J.-P. Chabriat, "Electrohydrodynamic force produced by a wire-to-cylinder dc corona discharge in air at atmospheric pressure," *Journal of Physics D: Applied Physics*, vol. 46, no. 47, p. 475204, 2013.

[22] D. S. Drew and K. S. J. Pister, "First takeoff of a flying microrobot with no moving parts," in *Manipulation, Automation and Robotics at Small Scales (MARSS), International Conference on,*. IEEE, 2017.

[23] W. Lindsay, D. Teasdale, V. Milanovic, K. Pister, and C. Fernandez-Pello, "Thrust and electrical power from solid propellant microrockets," in *MEMS*, 2001.

[24] D. J. Bell, T. Lu, N. A. Fleck, and S. M. Spearing, "Mems actuators and sensors: observations on their performance and selection for purpose," *Journal of Micromechanics and Microengineering*, vol. 15, no. 7, p. S153, 2005.

[25] R. Yeh, S. Hollar, and K. S. Pister, "Single mask, large force, and large displacement electrostatic linear inchworm motors," *Journal of Microelectromechanical Systems*, vol. 11, no. 4, pp. 330–336, 2002.

[26] I. Penskiy and S. Bergbreiter, "Optimized electrostatic inchworm motors," *J. Micromech. Microeng.*, vol. 23, 2013.

[27] D. S. Contreras and K. S. J. Pister, "Durability of Silicon Pin-Joints for Microrobotics," in *MARSS*, 2016.

[28] S. Hollar, a. Flynn, C. Bellew, and K. Pister, "Solar powered 10 mg silicon robot," *The Sixteenth Annual International Conference on Micro Electro Mechanical Systems, 2003. MEMS-03 Kyoto. IEEE*, pp. 706–711, 2003.

[29] D. S. Contreras, D. Drew, and P. K. S. J., "First steps of a millimeter-scale walking silicon robot," in *Solid State Sensors, Actuators, and Microsystems*, 2017, to appear in.

[30] B. G. Kilberg, D. S. Contreras, J. Greenspun, and K. S. J. Pister, "Mems aerodynamic control surfaces for millimeter-scale rockets," in *Manipulation, Automation and Robotics at Small Scales (MARSS), International Conference on*. IEEE, 2017, under review.

[31] C. L. Bellew, S. Hollar, and K. Pister, "An soi process for fabrication of solar cells, transistors and electrostatic actuators," in *TRANSDUCERS, Solid-State Sensors, Actuators and Microsystems, 12th International Conference on, 2003*, vol. 2. IEEE, 2003, pp. 1075–1078.

[32] Y. Khan, F. J. Pavinatto, M. C. Lin, A. Liao, S. L. Swisher, K. Mann, V. Subramanian, M. M. Maharbiz, and A. C. Arias, "Inkjet-printed flexible gold electrode arrays for bioelectronic interfaces," *Advanced Functional Materials*, 2015.

[33] R. Wood, S. Avadhanula, E. Steltz, M. Seeman, J. Entwistle, A. Bachrach, G. Barrows, S. Sanders, and R. Fearing, "Design, fabrication and initial results of a 2g autonomous glider," in *Industrial Electronics Society, 2005. IECON 2005. 31st Annual Conference of IEEE*. IEEE, 2005, pp. 8–pp.

[34] A. E. Ostfeld, A. M. Gaikwad, Y. Khan, and A. C. Arias, "High-performance flexible energy storage and harvesting system for wearable electronics," *Scientific reports*, vol. 6, 2016.

[35] G. Xue, M. Toda, and T. Ono, "Comb-drive xyz-microstage with large displacements based on chip-level microassembly," *Journal of Microelectromechanical Systems*, vol. 25, no. 6, pp. 989–998, 2016.

[36] R. V. Kulkarni and G. K. Venayagamoorthy, "Bio-inspired algorithms for autonomous deployment and localization of sensor nodes," *IEEE Transactions on Systems, Man, and Cybernetics, Part C (Applications and Reviews)*, vol. 40, no. 6, pp. 663–675, 2010.

[37] B. R. Donald, C. G. Levey, and I. Paprotny, "Planar microassembly by parallel actuation of mems microrobots," *Journal of Microelectromechanical Systems*, vol. 17, no. 4, pp. 789–808, 2008.

[38] A. Dementyev, H.-L. C. Kao, I. Choi, D. Ajilo, M. Xu, J. A. Paradiso, C. Schmandt, and S. Follmer, "Rovables: Miniature on-body robots as mobile wearables," in *Proceedings of the 29th Annual Symposium on User Interface Software and Technology*. ACM, 2016, pp. 111–120.

[39] J. McLurkin, J. Smith, J. Frankel, D. Sotkowitz, D. Blau, and B. Schmidt, "Speaking swarmish: Human-robot interface design for large swarms of autonomous mobile robots." in *AAAI spring symposium: to boldly go where no human-robot team has gone before*, 2006, pp. 72–75.